INTERIOR STRESS CALCULATIONS IN 2-D TIME-DOMAIN TRANSIENT BEM ANALYSIS

A. S. M. ISRAIL and P. K. BANERJEE

Department of Civil Engineering, State University of New York at Buffalo, 240 Ketter Hall, Buffalo, NY 14260, U.S.A.

Abstract—An improved and accurate formulation of time-domain BEM for determining the interior stresses in a 2-D transient dynamic analysis is presented. A new set of simpler and better behaved transient dynamic stress-kernels is derived. With these interior stress-kernels, it has been possible to overcome all the analytical complexities that have hindered the accurate determination of interior stresses in the past. The accuracy and stability are established via a few numerical examples, including those involving stress concentrations.

INTRODUCTION

The accurate determination of dynamic stresses remains one of the most difficult problems of engineering analysis. The Boundary Element Method (BEM) has proven to be one of the better numerical methods for stress analysis (Banerjee and Butterfield, 1981). However, for 2-D transient dynamic problems, because of the inherent complexity no attempt was made at deriving these integral identities for interior stresses for a long time. Instead, interior stresses were determined from interior displacements via a Finite Element type algorithm (Mansur, 1983). Only recently did Israil and Banerjee (1990) overcome these difficulties and derive them for the first time. However, it was later observed that there remained an apparent singularity at the wave-front in the convoluted form of these kernels which needed elaborate and expensive numerical treatment for some problems. Moreover, for fracture mechanics problems where the element sizes can vary rapidly over the surface, the results of the interior stresses obtained by the technique described in Israil and Banerjee (1990) were found to be inadequate. In this paper, those difficulties have been removed through some convenient condensation which makes the convoluted stress-kernels simpler to deal with and well behaved. It has been shown that the resulting analysis is capable of producing accurate solutions for problems with any kind of discretization pattern.

BOUNDARY INTEGRAL EQUATION

The boundary integral equation for time-domain transient dynamics can be expressed as (Banerjee and Butterfield, 1981):

$$c_{ij}(\xi)u_i(\xi, T) = \int_S [G_{ij}(x, T; \xi, \tau) * t_i(x, T) - F_{ij}(x, T; \xi, \tau) * u_i(x, T)] \, dS(x), \qquad (1)$$

where $u_i(x, T)$ = displacement; $t_i(x, T)$ = traction; T, the time at which response is desired; x and ξ are the field and source points respectively, and * indicates convolution integrals. G_{ij} and F_{ij} are, respectively, the displacement and traction-kernels in 2-D transient elastodynamics. They are given in Israil and Banerjee (1990) but are repeated here for completeness:

$$G_{ij} = \frac{1}{2\pi\rho} \left\{ \frac{1}{c_1} H\left(\frac{c_1 t'}{r} - 1\right) \left[\frac{2\left(\frac{c_1 t'}{r}\right)^2 - 1}{\sqrt{\left(\frac{c_1 t'}{r}\right)^2 - 1}} \left(\frac{r_i r_j}{r}\right) - \left(\frac{\delta_{ij}}{r}\right)\sqrt{\left(\frac{c_1 t'}{r}\right)^2 - 1} \right] \right.$$

$$\left. + \frac{1}{c_2} H\left(\frac{c_2 t'}{r} - 1\right) \left[-\frac{2\left(\frac{c_2 t'}{r}\right)^2 - 1}{\sqrt{\left(\frac{c_2 t'}{r}\right)^2 - 1}} \left(\frac{r_i r_j}{r}\right) + \left(\frac{\delta_{ij}}{r}\right)\frac{\left(\frac{c_2 t'}{r}\right)^2}{\sqrt{\left(\frac{c_2 t'}{r}\right)^2 - 1}} \right] \right\} \quad (2a)$$

$$F_{ij} = \frac{\mu}{2\pi\rho r} \left\{ \frac{1}{c_1} H\left(\frac{c_1 t'}{r} - 1\right) \left[\frac{1}{\left\{\left(\frac{c_1 t'}{r}\right)^2 - 1\right\}^{3/2}} \left(\frac{A_1}{r}\right) + \frac{2\left(\frac{c_1 t'}{r}\right) - 1}{\sqrt{\left(\frac{c_1 t'}{r}\right)^2 - 1}} \left(\frac{2A_2}{r}\right) \right] \right.$$

$$\left. - \frac{1}{c_2} H\left(\frac{c_2 t'}{r} - 1\right) \left[\frac{1}{\left\{\left(\frac{c_2 t'}{r}\right)^2 - 1\right\}^{3/2}} \left(\frac{A_3}{r}\right) + \frac{2\left(\frac{c_2 t'}{r}\right)^2 - 1}{\sqrt{\left(\frac{c_2 t'}{r}\right)^2 - 1}} \left(\frac{2A_2}{r}\right) \right] \right\} \quad (2b)$$

where $t' = T - \tau$ is the retarded time; A_1, A_2 and A_3 are functions of spatial terms and can be found in the Appendix.

BOUNDARY INTEGRAL EQUATION FOR INTERIOR STRESS

The boundary integral equation for interior stress can be written as:

$$\sigma_{ij}(\xi, T) = \int_S [G_{kij}^a * t_k - F_{kij}^a * u_k] \, dS(x) \quad (3)$$

where G_{kij}^a and F_{kij}^a are the interior stress-kernels.

These kernels are derived from the boundary kernels using the relations:

$$G_{kij}^a = \lambda \delta_{ij} \frac{\partial G_{km}}{\partial \xi_m} + \mu\left(\frac{\partial G_{kj}}{\partial \xi_i} + \frac{\partial G_{ki}}{\partial \xi_j}\right) \quad (4a)$$

$$F_{kij}^a = \lambda \delta_{ij} \frac{\partial F_{km}}{\partial \xi_m} + \mu\left(\frac{\partial F_{kj}}{\partial \xi_i} + \frac{\partial F_{ki}}{\partial \xi_j}\right). \quad (4b)$$

During the derivation, operations are done on the terms corresponding to each wave separately and satisfying the causality of each wave. For this purpose, the boundary kernels given by expressions (2a) and (2b) are written, alternately, as:

$$G_{ij} = \frac{1}{2\pi\rho} \left\{ \frac{1}{c_1} g_1 - \frac{1}{c_2} g_2 \right\} \quad (5a)$$

$$F_{ij} = \frac{\mu}{2\pi\rho r} \left\{ \frac{1}{c_1} f_1 - \frac{1}{c_2} f_2 \right\}, \quad (5b)$$

where

$$g_1 = \frac{2\left(\frac{c_1 t'}{r}\right)^2 - 1}{\sqrt{\left(\frac{c_1 t'}{r}\right)^2 - 1}}\left(\frac{r_{,i} r_{,j}}{r}\right) - \frac{\delta_{ij}}{r}\sqrt{\left(\frac{c_1 t'}{r}\right)^2 - 1} \quad \text{when} \quad \frac{c_1 t'}{r} > 1$$

$$= 0 \quad \text{when} \quad \frac{c_1 t'}{r} < 1$$

$$g_2 = \frac{2\left(\frac{c_2 t'}{r}\right)^2 - 1}{\sqrt{\left(\frac{c_2 t'}{r}\right)^2 - 1}}\left(\frac{r_{,i} r_{,j}}{r}\right) - \frac{\delta_{ij}}{r}\frac{\left(\frac{c_2 t'}{r}\right)^2}{\sqrt{\left(\frac{c_2 t'}{r}\right)^2 - 1}} \quad \text{when} \quad \frac{c_2 t'}{r} > 1$$

$$= 0 \quad \text{when} \quad \frac{c_2 t'}{r} < 1$$

$$f_1 = \frac{1}{\left\{\left(\frac{c_1 t'}{r}\right)^2 - 1\right\}^{3/2}}\left(\frac{A_1}{r}\right) + \frac{2\left(\frac{c_1 t'}{r}\right) - 1}{\sqrt{\left(\frac{c_1 t'}{r}\right)^2 - 1}}\left(\frac{2A_2}{r}\right) \quad \text{when} \quad \frac{c_1 t'}{r} > 1$$

$$= 0 \quad \text{when} \quad \frac{c_1 t'}{r} < 1$$

$$f_2 = \frac{1}{\left\{\left(\frac{c_2 t'}{r}\right)^2 - 1\right\}^{3/2}}\left(\frac{A_3}{r}\right) + \frac{2\left(\frac{c_2 t'}{r}\right) - 1}{\sqrt{\left(\frac{c_2 t'}{r}\right)^2 - 1}}\left(\frac{2A_2}{r}\right) \quad \text{when} \quad \frac{c_2 t'}{r} > 1$$

$$= 0 \quad \text{when} \quad \frac{c_2 t'}{r} < 1.$$

Following the procedure outlined before, the stress-kernels are derived using expressions (5) and are given by:

$$G^q_{kij} = \frac{\mu}{2\pi\rho r}\left\{ -\frac{1}{c_1}H\left(\frac{c_1 t'}{r} - 1\right)\left[\frac{1}{\left\{\left(\frac{c_1 t'}{r}\right)^2 - 1\right\}^{3/2}}\left(\frac{B_1}{r}\right) + \frac{2\left(\frac{c_1 t'}{r}\right)^2 - 1}{\sqrt{\left(\frac{c_1 t'}{r}\right)^2 - 1}}\left(\frac{2B_2}{r}\right)\right] \right.$$

$$\left. + \frac{1}{c_2}H\left(\frac{c_2 t'}{r} - 1\right)\left[\frac{1}{\left\{\left(\frac{c_2 t'}{r}\right)^2 - 1\right\}^{3/2}}\left(\frac{B_3}{r}\right) + \frac{2\left(\frac{c_2 t'}{r}\right)^2 - 1}{\sqrt{\left(\frac{c_2 t'}{r}\right)^2 - 1}}\left(\frac{2B_2}{r}\right)\right] \right\} \quad \text{(6a)}$$

and

$$
F_{kij}^q = \frac{\mu^2}{2\pi\rho r^2}\left\{-\frac{1}{c_1}H\left(\frac{c_1 t'}{r}-1\right)\left[\frac{1}{\left\{\left(\frac{c_1 t'}{r}\right)^2-1\right\}^{5/2}}\left(\frac{3E_1}{r}\right)-\frac{1}{\left\{\left(\frac{c_1 t'}{r}\right)^2-1\right\}^{3/2}}\left(\frac{2E_2}{r}\right)\right.\right.
$$

$$
\left.-\frac{2\left(\frac{c_1 t'}{r}\right)^2-1}{\sqrt{\left(\frac{c_1 t'}{r}\right)^2-1}}\left(\frac{4E_3}{r}\right)\right]
$$

$$
+\frac{1}{c_2}H\left(\frac{c_2 t'}{r}-1\right)\left[\frac{1}{\left\{\left(\frac{c_2 t'}{r}\right)^2-1\right\}^{5/2}}\left(\frac{3E_4}{r}\right)-\frac{1}{\left\{\left(\frac{c_2 t'}{r}\right)^2-1\right\}^{3/2}}\left(\frac{2E_5}{r}\right)\right.
$$

$$
\left.\left.-\frac{2\left(\frac{c_2 t'}{r}\right)^2-1}{\sqrt{\left(\frac{c_2 t'}{r}\right)^2-1}}\left(\frac{4E_3}{r}\right)\right]\right\}. \tag{6b}
$$

In the above expressions, B_1, B_2, B_3 and E_1, E_2, E_3, E_4, E_5 contain spatial terms only and can be found in the Appendix. These are non-convoluted forms of the explicit 2-D transient interior stress-kernels and are presented here for the first time.

CONVOLUTED INTERIOR STRESS-KERNELS

The field variables are assumed to vary linearly during a time step and expressed as:

$$
f_i(\mathbf{x}, \tau) = M_1(\tau)f_i^n(\mathbf{x})+M_2(\tau)f_i^{n-1}(\mathbf{x}) \tag{7}
$$

where $f_i(\mathbf{x},\tau)$ stands for the displacement or the traction variable and $M_1(\tau)$ and $M_2(\tau)$ are linear temporal shape functions, given by:

$$
M_1(\tau) = \frac{\tau-t_{n-1}}{\Delta t}, \quad M_2(\tau) = \frac{t_n-\tau}{\Delta t}, \quad t_{n-1}<\tau<t_n;
$$

where the subscripts 1 and 2 refer to the forward and backward temporal nodes respectively during a time step.

With the temporal discretization given by eqn (7), the convolution integral in eqn (3) yields:

$$
G_{kij}^q * t_k = \sum_{n=1}^{N}\left[t_i^n\int_{(n-1)\Delta T}^{n\Delta T}G_{kij}^q M_1(\tau)\,d\tau+t_i^{n-1}\int_{(n-1)\Delta T}^{n\Delta T}G_{kij}^q M_2(\tau)\,d\tau\right]
$$

$$
= \sum_{n=1}^{N}[t_i^n G_{kij_1}^{qN-n+1}+t_i^{n-1}G_{kij_2}^{qN-n+1}]. \tag{8}
$$

This expression, together with a similar expression for $F_{kij}^q * u_k$, transform eqn (3) into:

$$\sigma_{ij}^N = \sum_{n=1}^{N} \int_S [G_{kij_1}^{\sigma^{N-n+1}} t_i^n + G_{kij_2}^{\sigma^{N-n+1}} t_i^{n-1}) + (F_{kij_1}^{\sigma^{N-n+1}} u_i^n + F_{kij_2}^{\sigma^{N-n+1}} u_i^{n-1}], \tag{9}$$

where the terms in the parentheses are the convoluted interior stress-kernels and are stated below:

$$
\begin{aligned}
G_{kij_1}^{\sigma^{N-n+1}} = \frac{\mu}{2\pi\rho r} &\left[\frac{H(\alpha_1-1)}{c_1^2} \left\{ \frac{T}{\Delta T} \left[\frac{\alpha_1}{\beta_1}(B_1) - 2\alpha_1\beta_1(B_2) \right] \right. \right. \\
&+ \frac{r}{c_1\Delta T}\left[-\frac{1}{\beta_1}(B_1) + 2B_2(\tfrac{2}{3}\beta_1^3 + \beta_1) \right] \Big\} \\
&+ \frac{H(\alpha_2-1)}{c_2^2}\left\{ \frac{T}{\Delta T}\left[-\frac{\alpha_2}{\beta_2}(B_3) + 2\alpha_2\beta_2(B_2) \right] \right. \\
&\left. \left. + \frac{r}{c_2\Delta T}\left[\frac{1}{\beta_2}(B_3) - 2B_2(\tfrac{2}{3}\beta_2^3 + \beta_2) \right] \right\} \right]_{z=(N-n)\Delta T}^{z=(N-n+1)\Delta T}
\end{aligned}
\tag{10a}
$$

$$
\begin{aligned}
G_{kij_2}^{\sigma^{N-n+1}} = \frac{\mu}{2\pi\rho r} &\left[\frac{H(\alpha_1-1)}{c_1^2}\left\{ (1-T/\Delta T)\left[\frac{\alpha_1}{\beta_1}(B_1) - 2\alpha_1\beta_1(B_2) \right] \right. \right. \\
&\left. - \frac{r}{c_1\Delta T}\left[-\frac{1}{\beta_1}(B_1) + 2B_2(\tfrac{2}{3}\beta_1^3 + \beta_1) \right] \right\} \\
&+ \frac{H(\alpha_2-1)}{c_2^2}\left\{ (1-T/\Delta T)\left[-\frac{\alpha_2}{\beta_2}(B_3) + 2\alpha_2\beta_2(B_2) \right] \right. \\
&\left. \left. - \frac{r}{c_2\Delta T}\left[\frac{1}{\beta_2}(B_3) - 2B_2(\tfrac{2}{3}\beta_2^3 + \beta_2) \right] \right\} \right]_{z=(N-n)\Delta T}^{z=(N-n+1)\Delta T}
\end{aligned}
\tag{10b}
$$

$$
\begin{aligned}
F_{kij_1}^{\sigma^{N-n+1}} = \frac{\mu^2}{2\pi\rho r^2} &\left[\frac{H(\alpha_1-1)}{c_1^2}\left\{ (T/\Delta T)\left[-\frac{2\alpha_1^3-\alpha_1}{\beta_1^3}(E_1) - \frac{2\alpha_1}{\beta_1}(E_2) + 4\alpha_1\beta_1(E_3) \right] \right. \right. \\
&+ \frac{r}{c_1\Delta T}\left[-\frac{1}{\beta_1^3}(E_1) + \frac{2}{\beta_1}(E_2) - (\tfrac{4}{3}\beta_1^3 + 4\beta_1)E_3) \right] \Big\} \\
&+ \frac{H(\alpha_2-1)}{c_2^2}\left\{ (T/\Delta T)\left[\frac{2\alpha_2^3-3\alpha_2}{\beta_2^3}(E_4) + \frac{2\alpha_2}{\beta_2}(E_5) - 4\alpha_2\beta_2(E_3) \right] \right. \\
&\left. \left. + \frac{r}{c_2\Delta T}\left[\frac{1}{\beta_2^3}(E_4) - \frac{2}{\beta_2}(E_5) + (\tfrac{4}{3}\beta_2^3 + 4\beta_2)(E_3) \right] \right\} \right]_{z=(N-n)\Delta T}^{z=(N-n+1)\Delta T}
\end{aligned}
\tag{10c}
$$

$$
\begin{aligned}
F_{kij_2}^{\sigma^{N-n+1}} = \frac{\mu^2}{2\pi\rho r^2} &\left[\frac{H(\alpha_1-1)}{c_1^2}\left\{ (1-T/\Delta T)\left[-\frac{2\alpha_1^3-\alpha_1}{\beta_1^3}(E_1) - \frac{2\alpha_1}{\beta_1}(E_2) + 4\alpha_1\beta_1(E_3) \right] \right. \right. \\
&\left. - \frac{r}{c_1\Delta T}\left[-\frac{1}{\beta_1^3}(E_1) + \frac{2}{\beta_1}(E_2) - (\tfrac{4}{3}\beta_1^3 + 4\beta_1)E_3) \right] \right\} \\
&+ \frac{H(\alpha_2-1)}{c_2^2}\left\{ (1-T/\Delta T)\left[\frac{2\alpha_2^3-3\alpha_2}{\beta_2^3}(E_4) + \frac{2\alpha_2}{\beta_2}(E_5) - 4\alpha_2\beta_2(E_3) \right] \right. \\
&\left. \left. - \frac{r}{c_2\Delta T}\left[\frac{1}{\beta_2^3}(E_4) - \frac{2}{\beta_2}(E_5) + (\tfrac{4}{3}\beta_2^3 + 4\beta_2)(E_3) \right] \right\} \right]_{z=(N-n)\Delta T}^{z=(N-n+1)\Delta T},
\end{aligned}
\tag{10d}
$$

where

$$\alpha_i = \frac{c_i z}{r}$$

$$\beta_i = \sqrt{(\alpha_i)^2 - 1}.$$

The terms $1/\beta_1^3$ and $1/\beta_2^3$ appearing in eqns (10c) and (10d) have strong apparent singularity (of order $r^{-3/2}$) at the wave fronts. This apparent singularity does not seem to cause any trouble when the discretization contains elements of fairly uniform size. The difficulty occurs when one uses a model with widely varying elements, especially next to each other as is often needed in stress-concentration studies. However, this singularity is reduced if one adds the kernels corresponding to each time node together as discussed below.

Equation (9) can alternately be written as

$$\sigma_{ij}^N = \sum_{n=1}^{N} \int_S [(G_{kij_1}^{\sigma^{N-n+1}} + G_{kij_2}^{\sigma^{N-n}}) t_i^n + (F_{kij_1}^{\sigma^{N-n+1}} + F_{kij_2}^{\sigma^{N-n}}) u_i^n]. \tag{11}$$

In evaluating the kernels $(F_{kij_1}^{\sigma^{N-n+1}} + F_{kij_2}^{\sigma^{N-n}})$, the terms with apparent singularity of $r^{-3/2}$ at the wave-front vanish and only those with $r^{-1/2}$ singularity remain, the integration of which does not pose any difficulty. Thus the convoluted stress-kernels given by eqn (11), after convenient condensation, take the form:

$$G_{kij_1}^{\sigma^{N-n+1}} + G_{kij_2}^{\sigma^{N-n}} = \frac{\mu}{2\pi\rho r} \left[\frac{B_1}{c_1^2} P_1 - \frac{B_3}{c_2^2} P_2 + \tfrac{2}{3} B_2 \left(\frac{\Delta T}{r}\right)^2 (Q_2 - Q_1) \right] \tag{12a}$$

$$F_{kij_1}^{\sigma^{N-n+1}} + F_{kij_2}^{\sigma^{N-n}} = \frac{\mu^2}{2\pi\rho r^2} \left[\frac{-2(E_1 + E_2)}{c_1^2} P_1 + \frac{2(E_4 + E_5)}{c_2^2} P_2 \right.$$

$$\left. + \tfrac{4}{3} E_3 \left(\frac{\Delta T}{r}\right)^2 (Q_1 - Q_2) - \frac{E_1}{c_1^2} R_1 + \frac{E_4}{c_2^2} R_2 \right], \tag{12b}$$

where

$$P_\alpha = \sqrt{(N-n+1)^2 - \left(\frac{r}{c_\alpha \Delta T}\right)^2} - 2\sqrt{(N-n)^2 - \left(\frac{r}{c_\alpha \Delta T}\right)^2} + \sqrt{(N-n-1)^2 - \left(\frac{r}{c_\alpha \Delta T}\right)^2}$$

$$Q_\alpha = \left\{ (N-n+1)^2 - \left(\frac{r}{c_\alpha \Delta T}\right)^2 \right\}^{3/2} - 2 \left\{ (N-n)^2 - \left(\frac{r}{c_\alpha \Delta T}\right)^2 \right\}^{3/2}$$

$$+ \left\{ (N-n-1)^2 - \left(\frac{r}{c_\alpha \Delta T}\right)^2 \right\}^{3/2}$$

$$R_\alpha = \left(\frac{r}{c_\alpha \Delta T}\right)^2 \left[\frac{1}{\sqrt{(N-n+1)^2 - \left(\frac{r}{c_\alpha \Delta T}\right)^2}} - 2\frac{1}{\sqrt{(N-n)^2 - \left(\frac{r}{c_\alpha \Delta T}\right)^2}} \right.$$

$$\left. + \frac{1}{\sqrt{(N-n-1)^2 - \left(\frac{r}{c_\alpha \Delta T}\right)^2}} \right],$$

with $\alpha = 1, 2.$

These new forms of convoluted stress-kernels are, evidently, much simpler and better behaved than the previous ones. In evaluating the above terms the causality condition must always be satisfied, i.e. the time-related terms cannot be negative.

Once the time-convoluted kernels are sorted out as explained above, the numerical integration of eqn (11) is straightforward (Israil and Banerjee, 1990). Isoparametric quadratic elements are used for spatial modelling of the variables.

NUMERICAL EXAMPLES

The following examples are presented to demonstrate the capability of the interior stress algorithm to produce accurate solutions.

a. *Bar subjected to ramp-step load*

A ramp-step type of load (Fig. 2b) is applied to one end of a rectangular bar ($a/b = 2$), shown in Fig. 1, while the left end is fixed. The lateral sides are assumed to be traction-free. To simulate purely one-dimensional behavior, the Poisson's ratio of the material is assumed to be zero. This will facilitate comparison with available analytical solutions. For convergence studies, two types of mesh were chosen: one course mesh with 12 elements and another fine mesh with 48 elements (see Fig. 3). Axial stress is computed at 31 interior
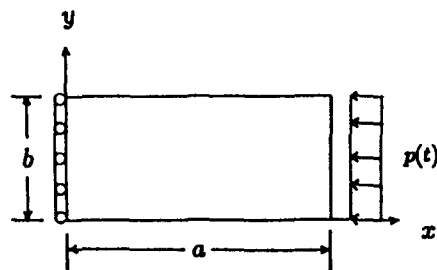
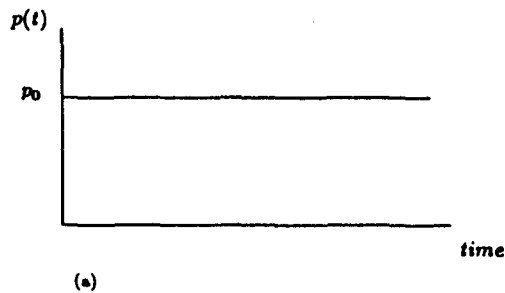Fig. 1. Rectangular bar ($a/b = 2$) with prescribed load and boundary conditions.
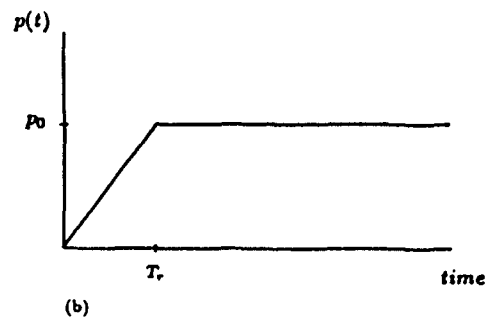
Fig. 2. Time history of prescribed load, (a) Heaviside type, and (b) ramp-step type.
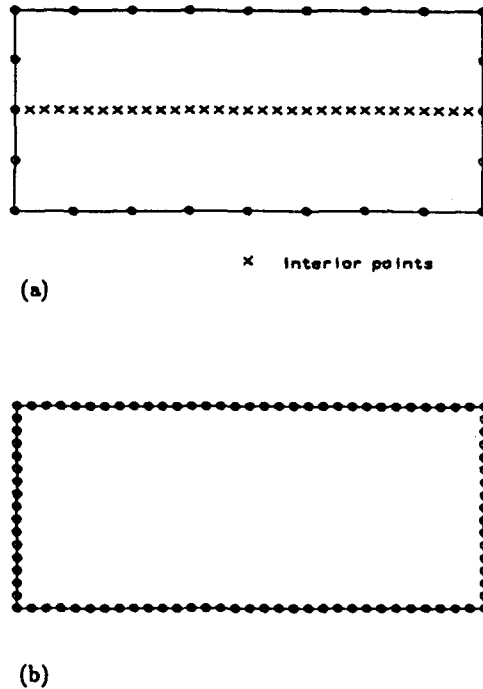
(a)

(b)

Fig. 3. Discretization of the bar, (a) coarse mesh (12 quadratic elements), and (b) fine mesh (48 quadratic elements).

points along the axis of the bar. The time response is studied using three cases: (a) coarse mesh with large time step, $\Delta T_1 = 0.125 a/c_1$; (b) coarse mesh with smaller time step, $\Delta T_2 = 0.03125 a/c_1$; and (c) fine mesh with smaller time step, $\Delta T_2 = 0.03125 a/c_1$. In each of the above cases, the responses are plotted at two different times: $T_1 = 0.5 a/c_1$ and $T_2 = 1.5 a/c_1$ and are presented in Figs 4, 5 and 6. The analytical solution shown is for a Heaviside-type load (Fig. 2a). The present algorithm with linear temporal variation of the field variables can model a ramp-type load better than a Heaviside-type one. Therefore, the sudden jump in the load is replaced by a ramp. The BEM solution shows a slope at the front of the wave and it is because of the ramp-type loading. It is observed that with coarse mesh and time-step ΔT_1 (P-wave travels 1/2 the element length during a time-step), there is some oscillation in the solution especially at time T_2 (Fig. 4). With smaller time-step ΔT_2 (P-wave travels 1/8th of the element length), the oscillation is reduced to a great extent as can be seen in Fig. 5. Oscillations disappear completely once a finer mesh with a compatible optimum time-step (P-wave travels 1/2 the element length) is used (Fig. 6). It has been observed that to obtain a given level of accuracy in interior stress, one needs a finer mesh than is needed for boundary solutions.

b. *Plate with a central crack*

Figure 7(a) shows the geometry and boundary conditions of a rectangular plate with a centrally located crack. It is loaded with a Heaviside-type step load. Because of symmetry, only one-quarter of the plate is modelled and the discretization is shown in Fig. 7(b). Two quarter-point elements are used one at each side of the crack-tip. This problem has been solved by Chen (1975) using a finite difference technique and later by Dominguez and Gallego (1989) who used traction-singular boundary elements. The plate-material is assumed to be linear elastic with the following parameters:

$$\text{shear modulus}, \mu = 76923 \text{ MPa},$$

$$\text{Poisson ratio}, \nu = 0.3,$$
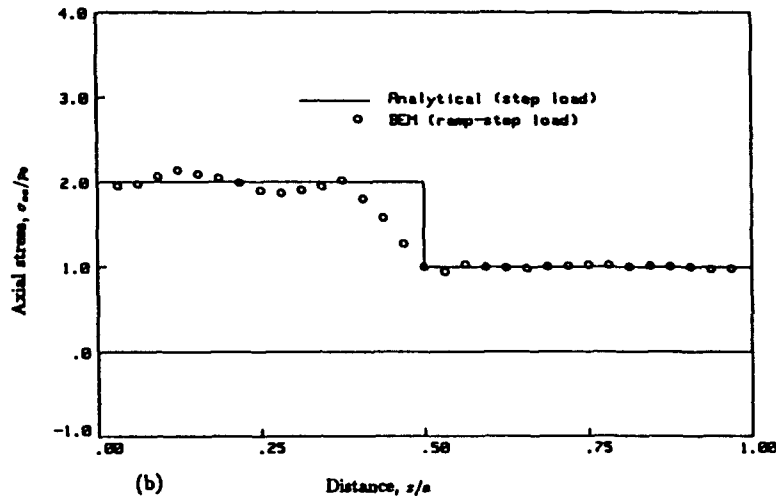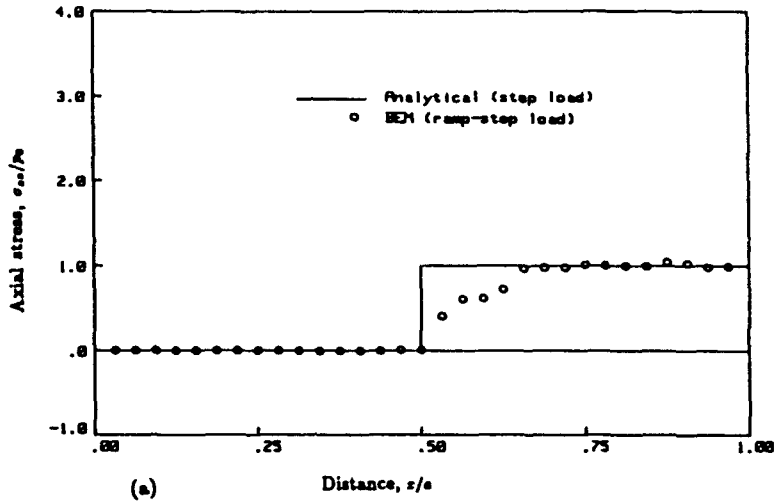
$$\text{density}, \rho = 5000 \text{ kg m}^{-3}.$$

Fig. 4. Interior stress. Coarse mesh with $\Delta T = 0.125a/c_1$, (a) at time $T_1 = 0.5a/c_1$, and (b) at time $T_2 = 1.5a/c_1$.
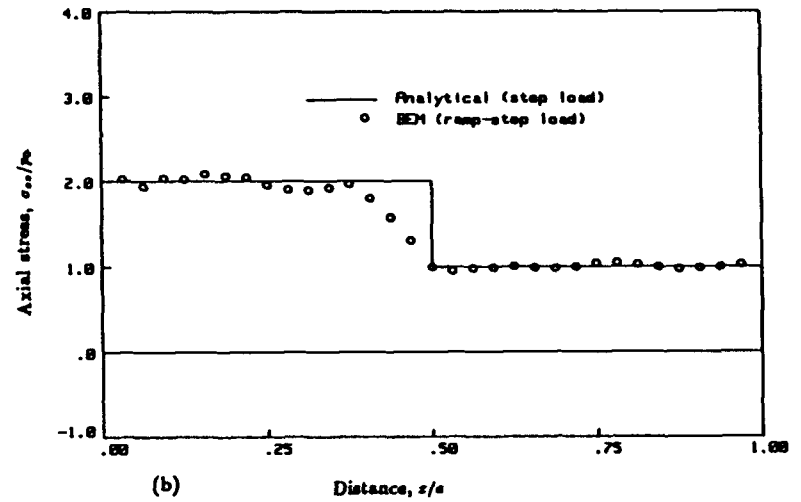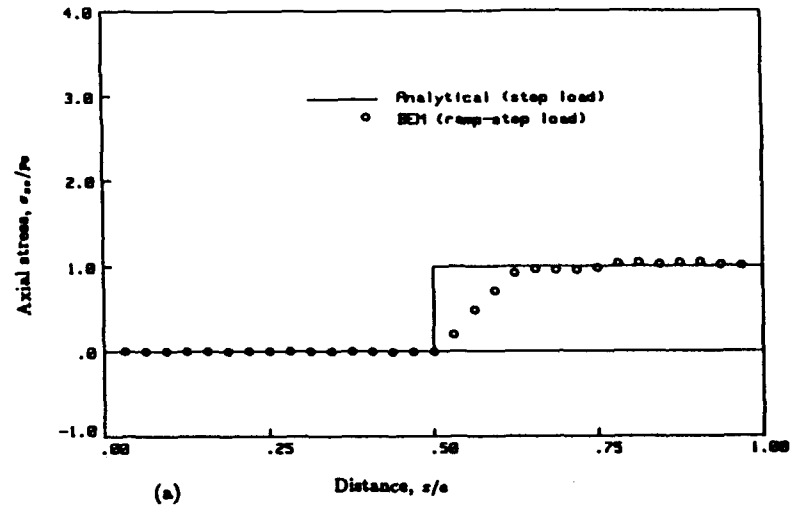

Fig. 5. Interior stress. Coarse mesh with $\Delta T = 0.03125a/c_1$, (a) at time $T_1 = 0.5a/c_1$, and (b) at time $T_2 = 1.5a/c_1$.
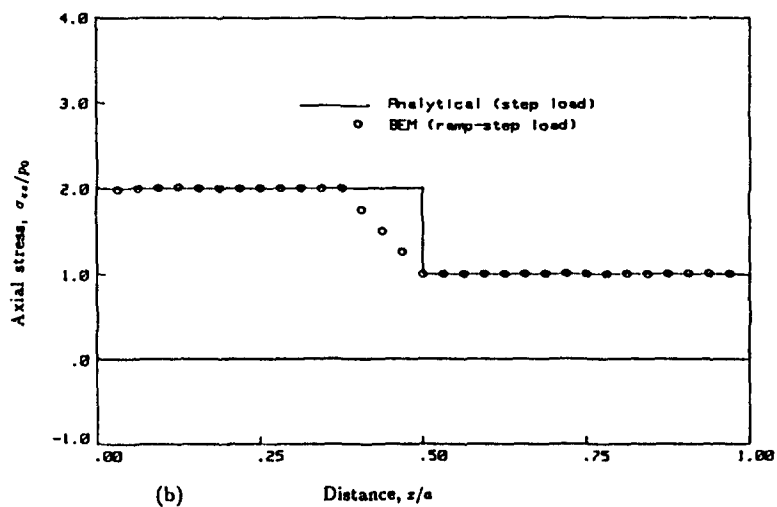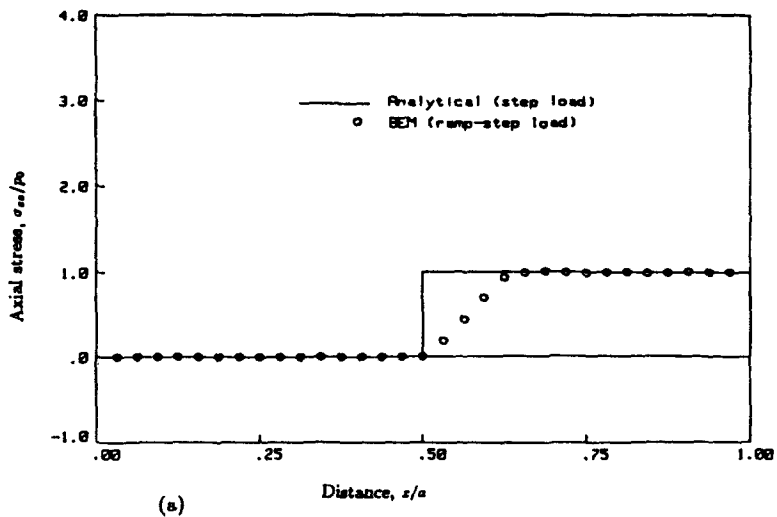
Fig. 6. Interior stress. Fine mesh with $\Delta T = 0.03125a/c_1$, (a) at time $T_1 = 0.5a/c_1$, and (b) at time $T_2 = 1.5a/c_1$.
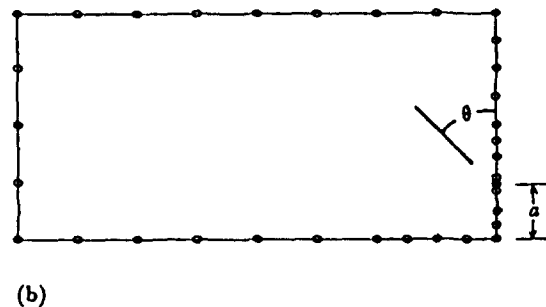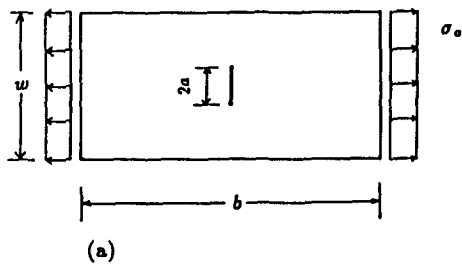

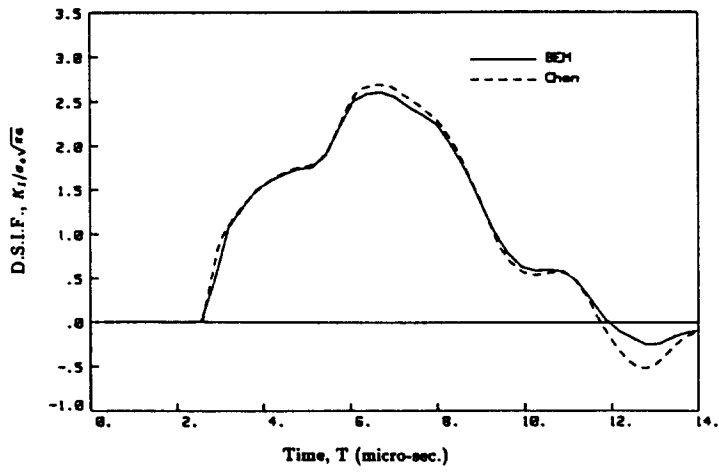Fig. 7. (a) Plate with a central crack, and (b) boundary discretization of 1/4th of the plate.

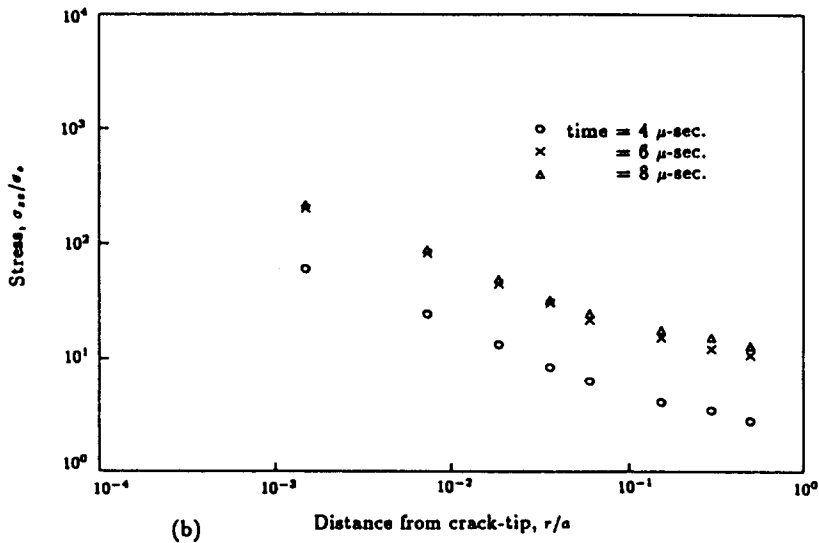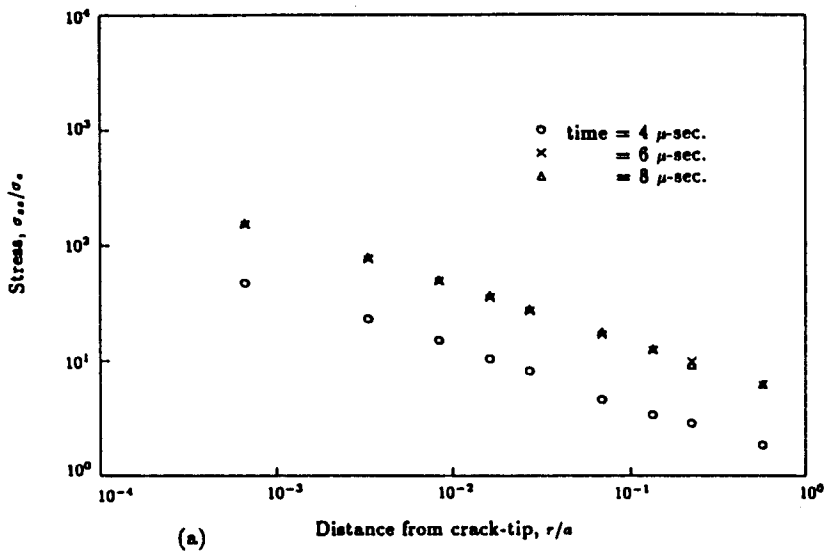Fig. 8. Comparison of dynamic stress intensity factors with published results.

(a)

(b)

Fig. 9. Interior stresses along (a) $\theta = 90^\circ$, and (b) $\theta = 45^\circ$.

The load intensity is:

$$\sigma_0 = 400 \text{ MPa}.$$

The various plate dimensions are:

$$\text{length, } b = 40 \text{ mm}$$

$$\text{width, } w = 20 \text{ mm}$$

$$\text{crack-length, } 2a = 4.8 \text{ mm}.$$

The time-step chosen is consistent with the element size and is taken as $\Delta T = 0.32 \ \mu$s, during which the P-wave travels about 2.4 mm.

The results obtained for the mode-I dynamic stress intensity factor (DSIF) by the present analysis are compared with those of Chen (1975) and are presented in Fig. 8. The DSIF are obtained from the crack opening displacements (COD) as described by Blandford *et al.* (1981) for static problems. Dominguez and Gallego (1989) obtained DSIF from crack-tip tractions (using traction-singular elements), and their results are almost identical to the present solutions in which no special traction-singular elements were used.

Interior stresses were obtained along lines inclined to the crack-axis at angles $\theta = 45°$ and 90° (Fig. 7b) leading to the crack-tip. The behavior of interior stresses in the vicinity of the crack-tip is $1/\sqrt{r}$, which in a logarithmic scale will show a linear variation. This phenomenon is depicted in Fig. 9 for various times where linear variations are noticed near the crack-tip but at greater distances, the variations are no longer linear.

CONCLUSION

An improved algorithm for determining transient dynamic stresses by time-domain BEM is presented. The non-integrable wave-front singularity in the interior stress-kernels is reduced to an integrable one. The resulting algorithm is capable of producing accurate solutions and has been demonstrated via numerical examples.

REFERENCES

Banerjee, P. K. and Butterfield, R. (1981). *Boundary Element Method in Engineering Science*. McGraw-Hill, London and New York.

Blandford, G. E., Ingraffea, A. R. and Liggett, J. A. (1981). Two-dimensional stress intensity factor computations using the boundary element method. *Int. J. Num. Meth. Engng* **17**, 387–404.

Chen, Y. M. (1975). Numerical computation of dynamic stress intensity factors by a Lagrangian finite-difference method (the Hemp-code). *Engng Fract. Mech.* **7**, 653–660.

Dominguez, J. and Gallego, R. (1989). Time domain boundary element analysis of two-dimensional crack problems. Proc. IABEM-89, United Technologies Research Center, Hartford, Connecticut.

Israil, A. S. M. and Banerjee, P. K. (1990). Advanced time-domain formulation of BEM for two-dimensional transient elastodynamics. *Int. J. Num. Meth. Engng* **29**, 1421–1440.

Mansur, W. J. (1983). A time-stepping technique to solve wave propagation problems using the boundary element method. Ph.D Thesis, Southampton University.

APPENDIX

(1) *Spatial terms in F-kernel*

$$A_1 = \frac{\lambda}{\mu} n_i r_{,j} + 2 r_{,i} r_{,j} \frac{\partial r}{\partial n}$$

$$A_2 = n_i r_{,j} + n_j r_{,i} + \frac{\partial r}{\partial n} (\delta_{ij} - 4 r_{,i} r_{,j})$$

$$A_3 = \frac{\partial r}{\partial n} (2 r_{,i} r_{,j} - \delta_{ij}) - n_j r_{,i}.$$

(ii) *Spatial terms in G" and F"-kernels*

$$B_1 = \frac{\lambda}{\mu} \delta_{ij} r_{,k} + 2 r_{,i} r_{,j} r_{,k}$$

$$B_2 = r_i \delta_{jk} + r_j \delta_{ik} + r_k \delta_{ij} - 4 r_i r_j r_k$$

$$B_3 = 2 r_i r_j r_k - r_i \delta_{jk} - r_j \delta_{ik}$$

$$E_1 = \left(\frac{\lambda}{\mu} \delta_{ij} + 2 r_i r_j \right) \left(\frac{\lambda}{\mu} n_k + 2 \frac{\partial r}{\partial n} r_k \right)$$

$$E_2 = -n_k \left[\frac{\lambda}{\mu} \delta_{ij} (2 + \lambda/\mu) + 2 r_i r_j \right] - 2 n_i r_j r_k - 2 n_j r_i r_k - 2 \frac{\partial r}{\partial n} (r_i \delta_{jk} + r_j \delta_{ik} + r_k \delta_{ij} - 6 r_i r_j r_k)$$

$$E_3 = n_i (-\delta_{jk} + 4 r_j r_k) + n_j (-\delta_{ik} + 4 r_i r_k) + n_k (-\delta_{ij} + 4 r_i r_j) + 4 \frac{\partial r}{\partial n} (r_i \delta_{jk} + r_j \delta_{ik} + r_k \delta_{ij} - 6 r_i r_j r_k)$$

$$E_4 = \frac{\partial r}{\partial n} (4 r_i r_j r_k - r_i \delta_{jk} - r_j \delta_{ik}) - n_i r_j r_k - n_j r_i r_k$$

$$E_5 = n_i (\delta_{jk} - 2 r_j r_k) + n_j (\delta_{ik} - 2 r_i r_k) - 2 n_k r_i r_j - 2 \frac{\partial r}{\partial n} (r_i \delta_{jk} + r_j \delta_{ik} + r_k \delta_{ij} - 6 r_i r_j r_k).$$